



—

Proceedings Book

**XI National and II International
Engineering Thermodynamics
Congress**

—

Albacete — 12-14 of June of 2019



**XI National and II International
Engineering Thermodynamics
Congress**

Albacete (Spain), Castilla-La Mancha University
from June 12th to 14th, 2019

Proceedings book

edited by: José A. Almendros Ibáñez
Antonio E. Molina Navarro
Juan F. Belmonte Toledo
Juan I. Córcoles Tendero

ISBN: 978-84-09-11635-5

Contents

| | |
|---|-------------|
| Contents | iii |
| Organization Committee | xiii |
| Scientific Committee | xv |
| Message from the Organization Committee | xix |
| 1 Energy efficiency and sustainability in buildings and industry | 1 |
| 1.1 28545. Estimation of the Heat Loss Coefficient for two houses through an average method | 3 |
| 1.2 28590. A sustainable pathway for the deployment of central solar heating plant coupled with seasonal storage in Spain | 15 |
| 1.3 28615. Innovative dynamic methodology for cost accounting and energy savings in building thermal systems | 27 |
| 1.4 28637. Simulation and optimization of a grid-integrated PV: A logistics center case study | 38 |
| 1.5 28653. Technical; economic and environmental feasibility of renewable-based energy systems in a Brazilian university hospital | 49 |
| 1.6 28852. Optimal design and operation of a multi-variable heat pump system for sanitary hot water production | 61 |
| 1.7 28927. Thermodynamic analysis of a high temperature heat pump coupled with an organic Rankine cycle for energy storage | 72 |
| 1.8 28976. Renewable Energies in Historical Buildings (REHIB project) | 84 |
| 1.9 28982. Artificial Lighting Data Acquisition in Buildings for BIM Integration Based on Computer Vision) | 92 |
| 1.10 28984. Building energy simulation using new interpolated forecast weather datasets) | 101 |
| 1.11 29064. Natural ventilation system in a residential dwelling assisted by solar chimney) | 112 |
| 1.12 29071. Assessing residential heating energy consumption in a city-scale: a bottom-up methodological approach) | 122 |

| | | |
|------|---|-----|
| 1.13 | 29101. A new improved CFD-based methodology to calculate the evaporation rate in indoor swimming pools) | 134 |
| 1.14 | 29102. Evaluation of correlations for the calculation of evaporation in unoccupied indoor pools) | 144 |
| 1.15 | 29395. Thermoelectric generator with passive heat exchangers for waste-heat recovery in a manufacturing plant) | 150 |
| 1.16 | 29411. Heat Pump control comparison of a conventional superheat system over a subcooling control system for Domestic Hot Water production) | 158 |
| 1.17 | 29412. Energy optimization of a thermal storage tank for Domestic Hot Water production) | 167 |
| 1.18 | 29848. Analysis of a PV Window for Building Integrated Photovoltaic (BIPV) Applications) | 176 |
| 1.19 | 30206. Experimental analysis of the refrigerant flow maldistribution in brazed plate heat exchangers) | 188 |
| 1.20 | 30401. Improving the energy efficiency of PCM based passive cooling system using natural ventilation) | 200 |
| 1.21 | 30402. Phase change material selection for two innovative compact energy storage systems in residential buildings) | 207 |
| 1.22 | 30494. State-of-the-art of high-temperature heat pumps for low-grade waste heat recovery) | 217 |
| 1.23 | 30495. Theoretical analysis of a small-scale and low-temperature Organic Rankine Cycle for a domestic Combined Heat and Power application) | 229 |
| 1.24 | 30496. Theoretical analysis of two-stage vapour compression cycle in high-temperature heat pumps for low-grade waste heat recovery) | 241 |
| 1.25 | 30661. Design and optimization of polygeneration systems for residential buildings integrating renewable energy; thermal energy storage and batteries considering legal restrictions) | 253 |
| 1.26 | 30668. Efficiency characterization of a variable speed compressor) | 265 |
| 1.27 | 30811. Experimental bench for energy storage by using phase-change materials (PCMs)) | 276 |
| 1.28 | 30941. Analysis and design of a solar parabolic trough - ORC - biomass poly-generation plant for a shopping centre) | 285 |
| 1.29 | 31129. Application of a building energy simulation methodology based on sensitivity analysis and Bayesian calibration to a PASLINK test cell case study) | 297 |
| 1.30 | 31130. Lighting performance assessing of road lighting installations based on the identification of the luminaires maintenance factor) | 305 |
| 1.31 | 31202. Indus3Es Project: Development of an Absorption Heat Transformer for waste heat revalorization in a petrochemical plant) | 312 |
| 1.32 | 31240. Thermal assessment of using passive PCM technology in lightweight buildings) | 321 |

Experimental analysis of the refrigerant flow maldistribution in braze plate heat exchangers

Lucas Álvarez-Piñeiro*¹, Paloma Albaladejo¹, Emilio Navarro-Peris¹, Lena Schnabel², Jose M. Corberán¹

*¹Instituto Universitario de Investigación de Ingeniería Energética (IUIIE), Universitat Politècnica de València, València, 46022, Spain

e-mail: lualpi@etsii.upv.es web: <http://www.iie.upv.es>

²Fraunhofer-Institut für Solare Energiesysteme ISE, Freiburg, Germany

ABSTRACT

Braze plate heat exchanger (BPHE) are used widely in heating and cooling systems and the efficiency of heat pumps depends critically on the proper performance of them. One of the most common factors affecting the performance of BPHE is the not uniform distribution of the refrigerant. This problem is especially important in the evaporator as the refrigerant enters in it in two phase flow and usually the distribution of liquid and vapor is not uniform over all the channels.

This problem is very well known in the literature, and manufacturers have implemented some technical solutions like introducing distributors in the inlet port in order to minimize this effect. Nevertheless, the applied solutions usually are developed only for the nominal conditions and when the BPHE work in other conditions is difficult to know which is going to be its behavior.

In this contribution, an experimental analysis of the refrigerant distribution in an evaporator BPHE as a function of the inlet and outlet conditions has been done. The BPHE has been tested working at several inlet conditions (quality) and outlet conditions (superheat) for different temperature difference in the secondary fluid and the refrigerant distribution inside the BPHE has been registered using thermography.

From the obtained results, it has been seen that: i) the flow maldistribution is present in most of the test, ii) the quality of the refrigerant at the inlet has an influence in the flow distribution, iii) the superheat has also a very important influence in the refrigerant maldistribution. In fact, the obtained results have shown that conditions working with low superheat show a better refrigerant distribution. Saturation temperature reduction at the evaporation seems to be a result of the refrigerant maldistribution. The COP degradation because of the refrigerant maldistribution is quite important for the performed test. In fact, it is important enough to remove any possible advantage derived for working at high superheat when the temperature lift in the water side is high.

Keywords: refrigerant maldistribution; brazed plate heat exchanger; thermography; BPHE

1. Introduction

The use of BPHEs for two-phase flow boiling was increasingly investigated within the last 10-15 years with the intention of using the high compactness and efficiency. Maldistribution was quickly observed as higher demands and bigger heat exchangers were needed. Evaporators are sensitive to uneven

distribution of liquid and vapor. Heat transfer is highly degraded in liquid-starved channels: heat transfer coefficient is lower for single-phase vapor flow regarding two-phase flow and as the refrigerant superheats, the temperature difference between refrigerant and the secondary fluid (e.g. water) reduces. Figure 1 shows the issue that this document is trying to understand. Furthermore, surface temperature is not distributed uniformly and can be observed by infrared thermography as shown in 2. Due to maldistribution, liquid or droplets can quite the evaporator and have an influence in the thermal expansion valve control. All these problems lead to a degradation in the performance of the system i.e. significant reductions in cooling capacity and COP.

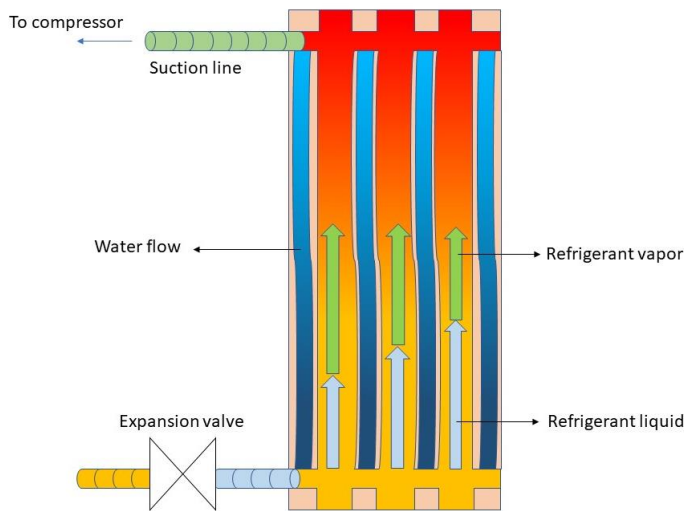


Figure 1. Uneven distribution of refrigerant in a heat exchanger

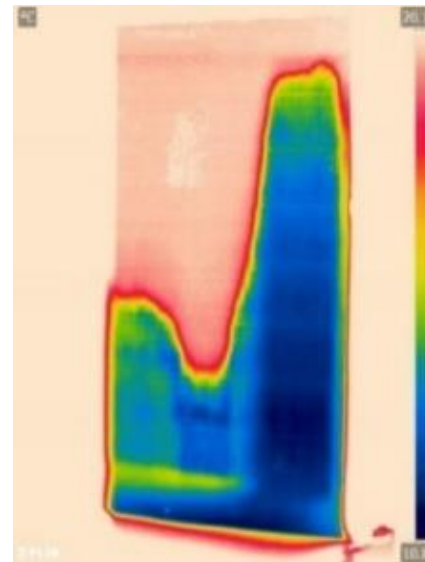


Figure 2. Thermography picture

From the early literature on the plates arrangements on flow distribution is presented [1, 2] where results indicate that manifold diameter and number of channels have great influence in maldistribution. Maldistribution causes higher or lower thermal performance degradation depending on if it is a U-type or Z-type heat exchanger. Z-type plate arrangement have more tendency to suffer maldistribution [12].

The quality distribution in heat exchanger manifolds were investigated [14] and thermal performance can be reduced due to liquid/vapor maldistribution. From their observations, vapor is taken out in the first channels when the inlet quality was low ($x=0.11$) but distributes evenly in the first channels when quality increased. However, no mention about the superheat in the evaporator is made.

Mass flow, flow pattern and inlet quality are variables to take into account to have mass flow evenly distributed within the channels. For high mass flow and low inlet quality, better distribution is mentioned by many researchers [4,8]. However, depending on the flow pattern better or less distribution is observed. Flow visualization before entering the evaporator recognized two patterns: churn and separated flow. Churn flow is recommended as liquid and vapor phase are homogeneously mixed whereas in separated flow, the different layers of vapor and liquid are perfectly separated [15].

For achieving better refrigerant distribution, many authors and companies proposed some solutions. There are distribution devices e.g. SWEP [11] developed a reliable system that feeds homogeneously with refrigerant all channels ensuring highly efficient heat transfer. For microchannel heat exchangers, [7] proposed an improvement for achieving better refrigerant distribution. The solution consisted in remove flash gas; vapor phase is separated from liquid phase after the expansion valve. In this way, only liquid is flowing within the microchannel heat exchanger while the vapor phase is being bypassed. Thermography pictures showed clear more uniformly distributed superheat with this flash gas removal system. Furthermore, better system performance was observed when using the separation device. However, 0K superheat test was not performed. Although quality maldistribution can be avoided, further

studies observed that the outlet header pressure drop is the causes the mass flow rate to be different from tube to tube [13].

Infrared thermography is used by authors, as mentioned before, to study this phenomenon because it is non-intrusive and non-contacting, hence easy to apply. [3, 9] used thermography to visualize the two-phase flow region for different outlet vapour qualities and superheats of 5 and 10 K and to outline a methodology to quantify both refrigerant maldistribution and effective usage of the heat exchanger respectively.

Nevertheless, the influence of different process conditions like superheat or the temperatures difference at the secondary fluid for the two-phase flow evaporation is not addressed in open literature. In order to understand the reasons more deeply a measurement campaign was designed and performed to analyse experimentally the refrigerant distribution in a BPHE changing inlet and outlet conditions, thus inlet quality and superheat for a given secondary temperature difference, to understand dependencies and reasons for the behaviour in the evaporator. Uneven temperature distribution in the surface is a result of non-uniform refrigerant distribution within the channels and can be registered with a thermography camera.

2. Experimental set-up

The test rig, a water-to-water heat pump booster prototype with propane (R290) as refrigerant for heat recovery applications. The test rig permits to work with and without superheat and different levels of subcooling, giving the choice to change the quality at the entry. Therefore, two working modes are available, with superheat (mode 1) and without superheat (mode 2).

When working with superheat, two expansion devices are operating: a throttling valve, located between the condenser and the liquid receiver, and an expansion valve, placed between the liquid receiver and the evaporator. The liquid receiver is used to accommodate the changes in the active charge in the system derived from the variations in the degree of subcooling at the condenser. In figure 3 the scheme of the water-to-water heat pump to make subcooling in the condenser is shown. The throttling valve is the active control component that allows setting the subcooling at the condenser independently from the external conditions (point 3). Therefore, a change in the pressure drop in the valve will produce a change in the subcooling at the outlet of the condenser. The liquid receiver ensures that the refrigerant leaves throttling valve in saturated liquid state (point 4). Measuring pressure at the liquid receiver allows knowing the quality at the entry of the evaporator (point 5), as the pressure is measured in point 1. Pressure drop at the evaporator is not measured. However, when no superheat is not used (SH= 0 K), the liquid receiver is bypassed and only the

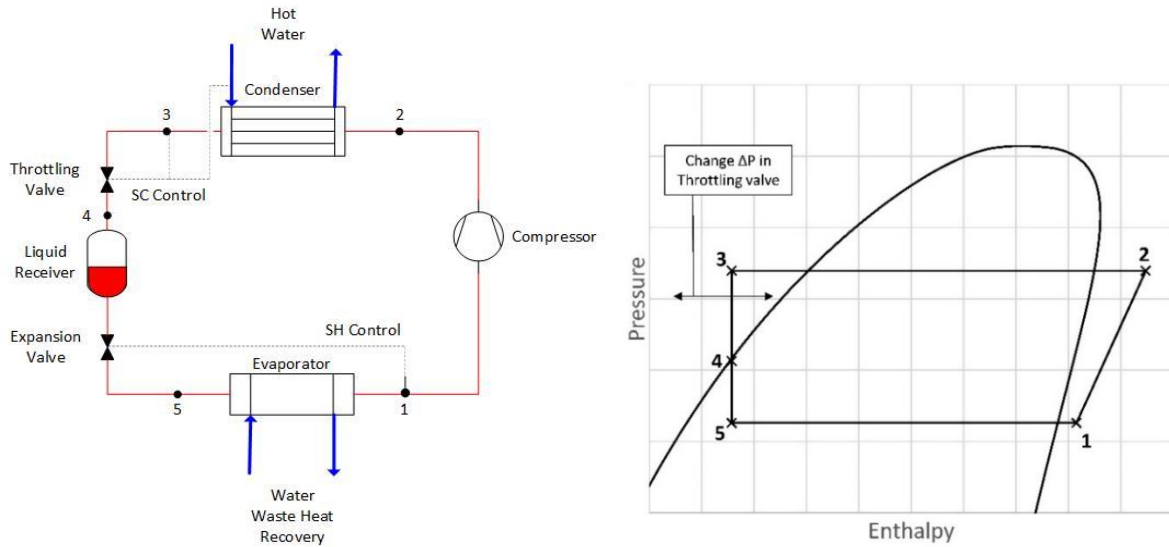


Figure 3. Mode 1 configuration system lay-out and refrigerant cycle

When working in mode 2, without superheat, the expansion valve is dedicated to control the subcooling at the expense of losing the superheat control. In this sense, the liquid receiver is placed at the outlet of the evaporator (point 5) ensuring saturated vapor conditions at compressor inlet (zero superheat). The evaporation pressure depends mainly on the heat process at the evaporator (points 4-5) while the condensing pressure is constrained from the heat process in the condenser (points 2-3). The pressure drop introduced by the expansion valve will determine the degree of subcooling produced at the condenser.

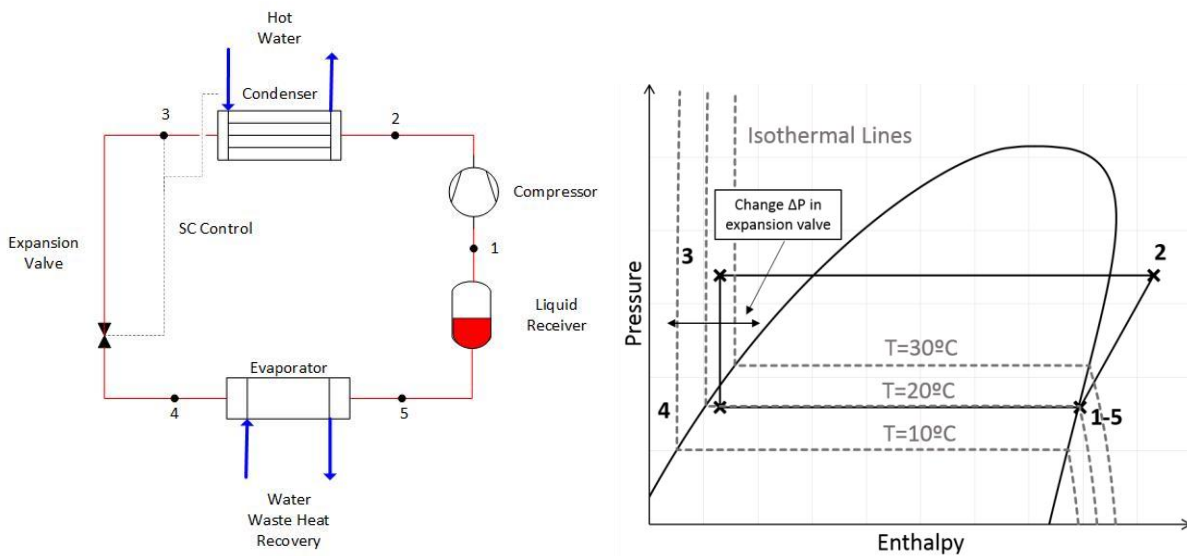


Figure 4. Mode 2 configuration: system lay-out and refrigerant cycle

In figure 5, the green box is the unit to be tested, more concretely the inlet/outlet of the BHPE. A frequency variable water pump adjusts the water mass flowrate, which will determine the temperature at the outlet of the evaporator. For more information please refer to [10].

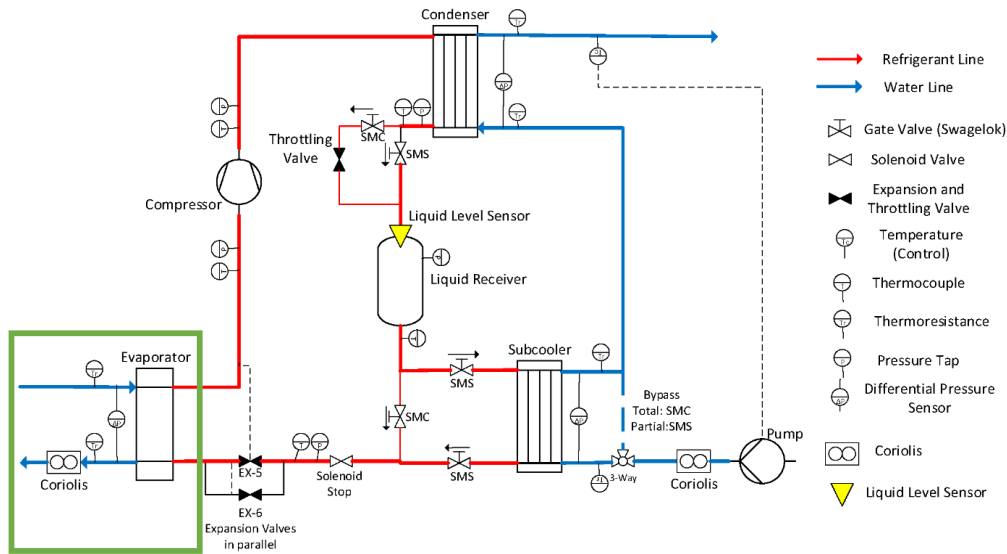


Figure 5. Propane Water-to-water heat pump booster.

The evaporator is the model AC-70X-120M from Alfa Laval. 40 kW capacity at the nominal point, 120 plates and a horizontal port distance and vertical port distance of 50 mm and 466 mm respectively resulting a 6 m² heat transfer area.

A thermoresistance is on each side of the evaporator and the water mass flow is measured with a Coriolis mass flow meter. For the pressure on the refrigerant side, three Rosemount sensors are installed. In order to monitor and measure the parameters on the BHPE, all the sensors were connected to a data acquisition system “Agilent 34970A”, where all parameters were monitored.

The relative and absolute accuracy of each device are shown in the following table:

Table 1. Instrumentation used in the test rig

| Magnitude | Model | Relative accuracy | Absolute accuracy |
|-------------|-----------------------------------|-------------------|-------------------|
| Pressure | P 1151 Smart GP7 Rosemount | 0.12 % of Span | 0.03 |
| | P 1151 Smart GP8 Rosemount | 0.15 % of Span | 0.08 |
| | P 3051 TG3 Rosemount | 0.14 % of Span | 0.04 |
| Temperature | RTD Class 1/10 DIN | | 0.06 |
| Mass Flow | Coriolis SITRANS F C MASS 2100 | 0.3 % of Reading | |

3. Performed test

Based on the pre-evaluation and literature research on the relevant aspects a field of operation points was defined and characterized experimentally. The following values were varied:

- superheat at the evaporator (0K/ 5 K/ 10 K/ 15K)

- inlet quality (0,06/ 0,14/ 0,2/ 0,3)
- temperature difference at the secondary fluid (5 K and 13 K)

The chosen values correspond to regular inlet qualities ($0.14 < x < 0.3$) and superheat (5-15 K) in heat pump applications. As the test rig can work in numerous levels of subcooling without interfering superheat, 0 K superheat and an unusual inlet quality of 0,06 in the evaporator is suggested to cover the measurement campaign. Evaporation temperature has been registered for each case.

The matrix concludes different superheats at different inlet qualities at a temperature difference of 5 K and 13 K at the secondary fluid as it can be seen in figure 3:

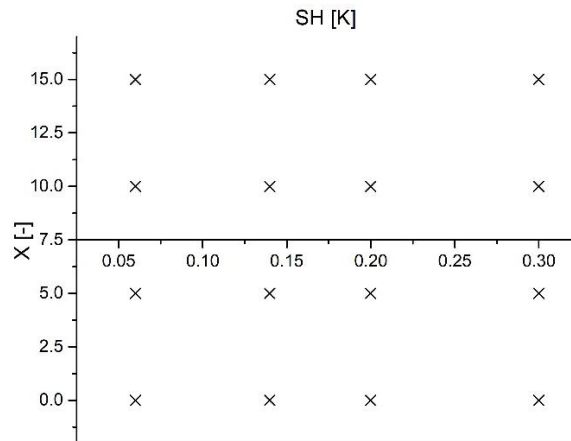


Figure 6. Experimental measures points for $dT_{water} = 5$ K and $dT_{water} = 13$ K

To register the refrigerant distribution, the surface of the evaporator is been photographed by IR thermography. Qualitative thermography tests are performed, this means that we are comparing different point's temperature but not measuring temperature accurately. The IR camera was set to a measuring range of -40 to 120°C. In the next figure, a picture of a frontal view of the evaporator (face used for thermography) and a transversal view with the location of the refrigerant and water inlet/outlet ports.

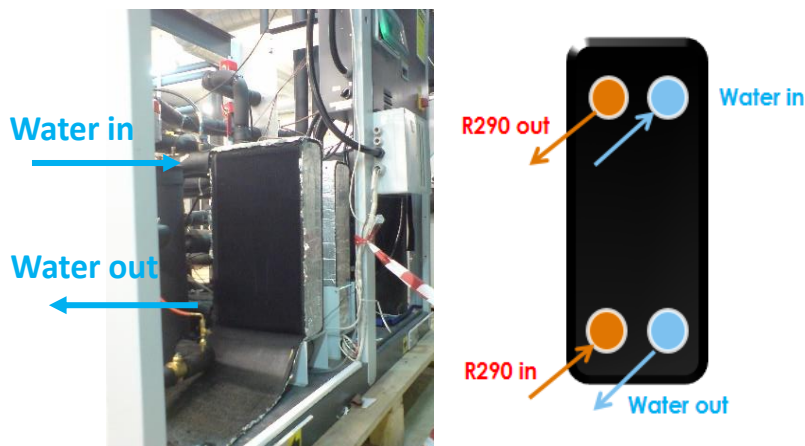
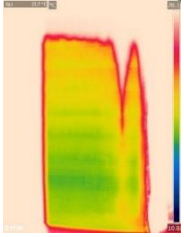
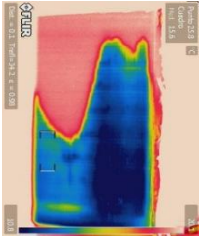
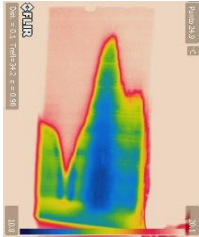

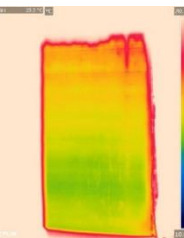
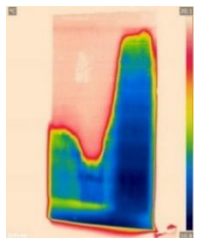
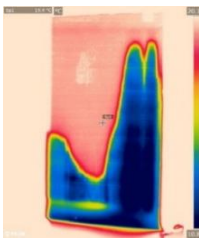
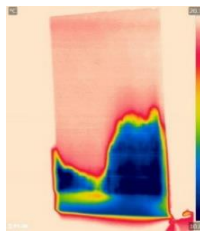
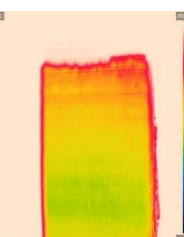
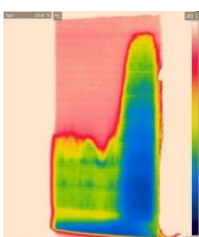
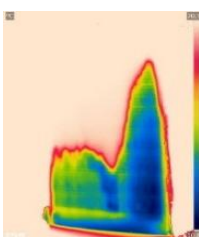
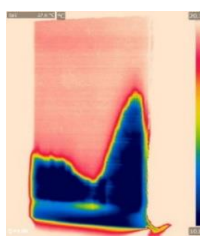
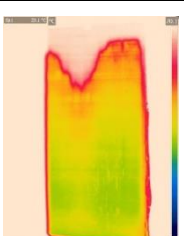
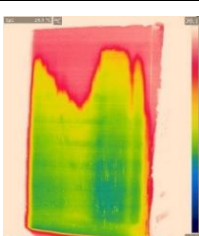
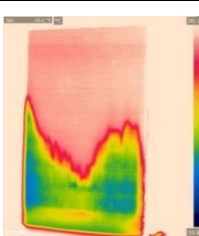
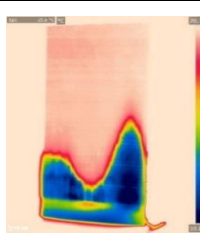


Figure 7. Picture of a frontal view of the evaporator and a transversal view with the location of the inlet/outlet ports

The next table shows the corresponding IR thermographies for a water temperature difference of 5 K. They are given in tables in the corresponding order of superheats. The minimum temperature of the scale is set to 10,8°C and the maximum to 20,1°C. This means that temperatures below and around

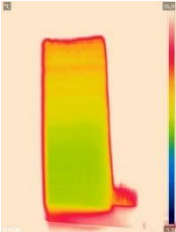
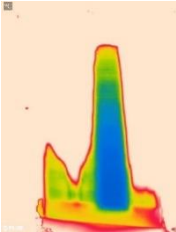
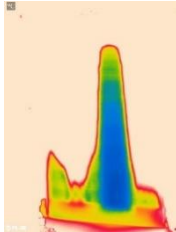
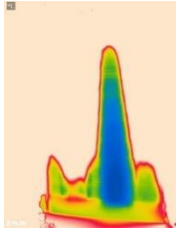
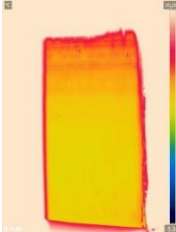
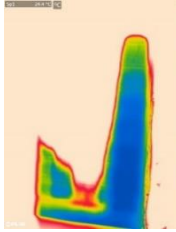
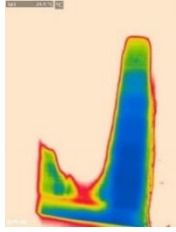
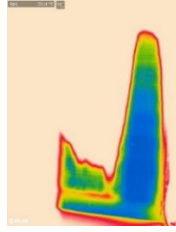
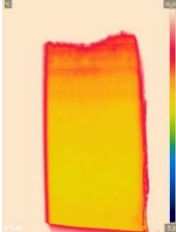
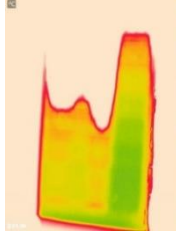
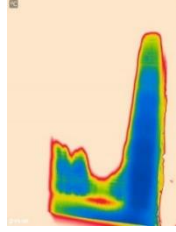
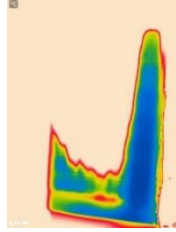


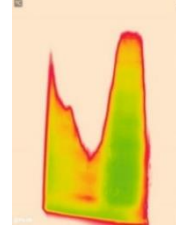
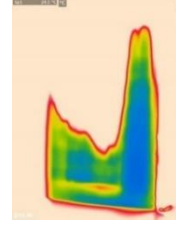
10,8°C is shown in dark-blue whereas bright colours are for intermediate temperature. Red are for temperatures near 20,1°C and white for temperatures above. The following aspects can be clearly stated.

Table 2. Thermographies for $dT_{\text{water}}= 5 \text{ K}$ with variation of inlet quality and superheat

| $dT_{\text{water}}= 5\text{K}$ | SH= 0 K | SH= 5K | SH= 10 K | SH= 15 K |
|--------------------------------|---|--|--|--|
| x=0.06 |  <p>$T_{\text{evap}}= 12.34 \text{ }^{\circ}\text{C}$ $DT_{\text{evap}}= 5.26$ $x=0.053$</p> |  <p>$T_{\text{evap}}= 10.34 \text{ }^{\circ}\text{C}$ $DT_{\text{evap}}= 4.58$ $x=0.078$</p> |  <p>$T_{\text{evap}}= 9.00 \text{ }^{\circ}\text{C}$ $DT_{\text{evap}}= 5.17$ $x=0.085$</p> |  <p>$T_{\text{evap}}= 4.61 \text{ }^{\circ}\text{C}$ $DT_{\text{evap}}= 5.3$ $x=0.068$</p> |
| x=0.14 |  <p>$T_{\text{evap}}= 12.81 \text{ }^{\circ}\text{C}$ $DT_{\text{evap}}= 5.22$ $x=0.142$</p> |  <p>$T_{\text{evap}}=8.37^{\circ}\text{C}$ $DT_{\text{evap}}= 5.4$ $x=0.141$</p> |  <p>$T_{\text{evap}}=7.39^{\circ}\text{C}$ $DT_{\text{evap}}= 5.3$ $x=0.141$</p> |  <p>$T_{\text{evap}}=4.61^{\circ}\text{C}$ $DT_{\text{evap}}= 4.9$ $x=0.142$</p> |
| x=0.20 |  <p>$T_{\text{evap}}= 13.21 \text{ }^{\circ}\text{C}$ $DT_{\text{evap}}= 4.85$ $x=0.199$</p> |  <p>$T_{\text{evap}}=10.01^{\circ}\text{C}$ $DT_{\text{evap}}= 4.3$ $x=0.191$</p> |  <p>$T_{\text{evap}}=8.42^{\circ}\text{C}$ $DT_{\text{evap}}= 4.9$ $x=0.185$</p> |  <p>$T_{\text{evap}}=4.8^{\circ}\text{C}$ $DT_{\text{evap}}= 5.1$ $x=0.208$</p> |
| x= 0.3 |  <p>$T_{\text{evap}}= 13.34 \text{ }^{\circ}\text{C}$ $DT_{\text{evap}}= 4.859$ $x=0.305$</p> |  <p>$T_{\text{evap}}=12.71^{\circ}\text{C}$ $DT_{\text{evap}}= 4.6$ $x=0.322$</p> |  <p>$T_{\text{evap}}=9.50^{\circ}\text{C}$ $DT_{\text{evap}}= 4.6$ $x=0.289$</p> |  <p>$T_{\text{evap}}=4.92^{\circ}\text{C}$ $DT_{\text{evap}}= 4.8$ $x=0.303$</p> |

Similar to the above mentioned, the next table shows the corresponding IR thermographies for a water temperature difference of 13 K. They are given in tables in the corresponding order of superheats. The minimum temperature of the scale is set to -5°C and the maximum to 16°C . If the previous scale were used, no bright colours were distinguished, only a dark-blue frame.

Table 3. Thermographies for $dT_{\text{water}} = 13 \text{ K}$ with variation of inlet quality and superheat

| $dT_{\text{water}} = 13 \text{ K}$ | SH= 0 K | SH= 5K | SH= 10 K | SH= 15 K |
|------------------------------------|---|---|--|--|
| $x=0.06$ |  $T_{\text{evap}} = 4.05 \text{ }^{\circ}\text{C}$ $DT_{\text{evap}} = 12.9$ $x=0.042$ |  $T_{\text{evap}} = -1.02 \text{ }^{\circ}\text{C}$ $DT_{\text{evap}} = 13.2$ $x=0.064$ |  $T_{\text{evap}} = -1.8 \text{ }^{\circ}\text{C}$ $DT_{\text{evap}} = 12.9$ $x=0.069$ |  $T_{\text{evap}} = -1.88 \text{ }^{\circ}\text{C}$ $DT_{\text{evap}} = 12.9$ $x=0.072$ |
| $x=0.14$ |  $T_{\text{evap}} = 5.9 \text{ }^{\circ}\text{C}$ $DT_{\text{evap}} = 13.04$ $x=0.142$ |  $T_{\text{evap}} = -2.02 \text{ }^{\circ}\text{C}$ $DT_{\text{evap}} = 13.1$ $x=0.139$ |  $T_{\text{evap}} = -2.46 \text{ }^{\circ}\text{C}$ $DT_{\text{evap}} = 13$ $x=0.139$ |  $T_{\text{evap}} = -1.88 \text{ }^{\circ}\text{C}$ $DT_{\text{evap}} = 13$ $x=0.141$ |
| $x=0.20$ |  $T_{\text{evap}} = 6.14^{\circ}\text{C}$ $DT_{\text{evap}} = 12.88$ $x=0.198$ |  $T_{\text{evap}} = -1.43 \text{ }^{\circ}\text{C}$ $DT_{\text{evap}} = 12.7$ $x=0.209$ |  $T_{\text{evap}} = -2.08 \text{ }^{\circ}\text{C}$ $DT_{\text{evap}} = 12.5$ $x=0.215$ |  $T_{\text{evap}} = -2.31 \text{ }^{\circ}\text{C}$ $DT_{\text{evap}} = 12.77$ $x=0.199$ |
| $x= 0.3$ |  $T_{\text{evap}} = 6.02 \text{ }^{\circ}\text{C}$ $DT_{\text{evap}} = 13$ $x=0.295$ |  $T_{\text{evap}} = 4.8 \text{ }^{\circ}\text{C}$ $DT_{\text{evap}} = 13.1$ $x=0.291$ |  $T_{\text{evap}} = 3.67^{\circ}\text{C}$ $DT_{\text{evap}} = 13.2$ $x=0.304$ |  $T_{\text{evap}} = -0.43 \text{ }^{\circ}\text{C}$ $DT_{\text{evap}} = 13.1$ $x=0.268$ |

The following aspects can be clearly stated from the thermography pictures presented in table 4 and table 5:

- The two-phase flow region can be identified by a sharp red line.
- For operation with superheat points, the two-phase flow region is not even distributed, indicating a maldistribution of the refrigerant mass flow. The right or the central part of the heat exchanger is shown to be occupied by two-phase flow. This indicates a higher mass flow rate in this part of the heat exchanger.
- The inlet quality influences the distribution. A higher inlet quality leads to a more even distribution of the two-phase flow region. However, higher inlet quality seems to not improve distribution for $dT_{\text{water}} = 13 \text{ K}$.
- For higher superheats the two-phase flow area is smaller than for lower superheats, the same superheat can be assumed for all channels.
- For lower superheat and inlet qualities the two-phase flow of the right part of the heat exchanger occupies the whole length of the channel. There the required superheat is probably not reached.
- Optimum refrigerant distribution is achieved when no superheat is performed although vapor is entering. As outlined in [7], this were only possible when no vapor was entering. Hence, further tests should be done with only liquid entering in the BPHE.

Nevertheless, the pressure difference between the low-pressure side (evaporator) and the high-pressure side (condenser) should be as small as possible to reduce energy consumption in the compressor. The higher the evaporation temperature, the higher the refrigerant density. Therefore, for each stroke the compressor can transport more refrigerant. Lower consumption and higher capacity will increase the total system efficiency.

The evaporation process needs the most heat transfer area of the evaporator. A BPHE which is forced to work with a high level of superheat will have less heat transfer area available for evaporation. Therefore, evaporation temperature decreases and leads to both system capacity and efficiency degradation.

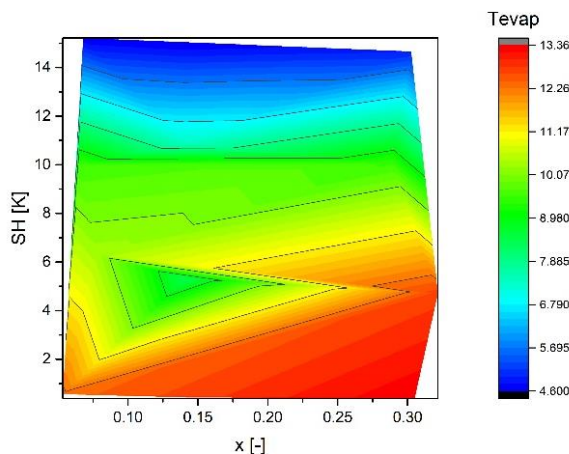


Figure 4. Saturation temperature for $dT_{\text{water}} = 5 \text{ K}$

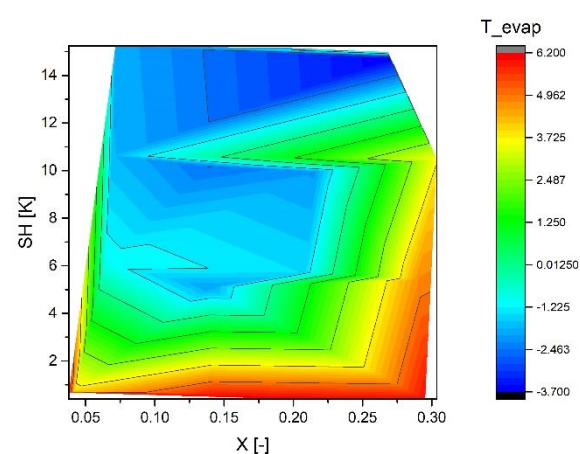


Figure 5. Saturation temperature for $dT_{\text{water}} = 13 \text{ K}$

It can be observed in figure 4 and figure 5 the evaporation temperature by plotting it as a function of superheat and inlet quality. In these figures the effect of maldistribution cannot be clearly observed as the influence of superheat and quality is present. Therefore, it is necessary to remove the effects due to thermodynamics.

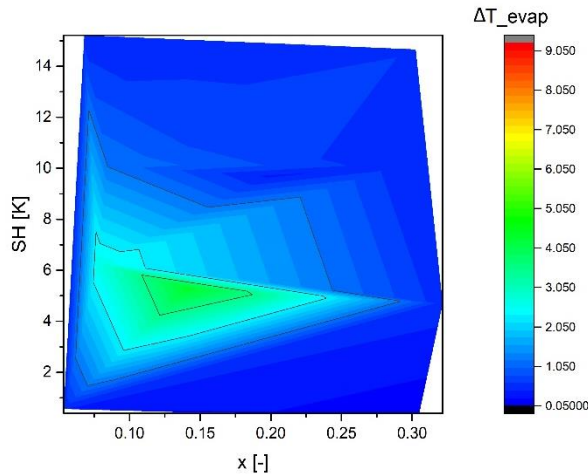


Figure 6. Absolute T_{evap} difference for $dT_{\text{water}}= 5$ K

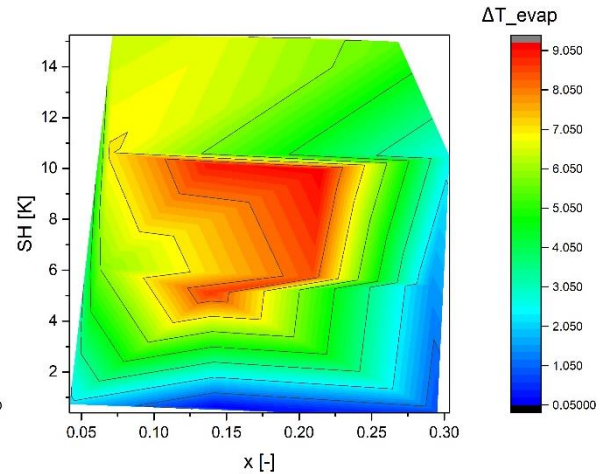


Figure 7. Absolute T_{evap} difference for $dT_{\text{water}}= 13$ K

In order to measure the effect of the maldistribution in the evaporation temperature and diminish the effect of thermodynamics (superheat and inlet quality), a software is used to obtain theoretical evaporation temperatures. The evaporator can be studied using the commercial software IMST-ART (IMST-ART v.3.90) [5]. IMST-ART is able to consider geometrical and operational parameters of evaporators in its global solution method called SEWTLE (Semi-Explicit method for Wall Temperature Linked Equations) [6].

Data from the experiments, inlet conditions (quality, refrigerant mass flow, water mass flow and water inlet temperature) and exit conditions (superheat), is introduced in the software. The theoretical evaporation temperature is compared with the experimental evaporation temperature in figures 6 and 7 for $dT_{\text{water}}= 5$ K and $dT_{\text{water}}= 13$ K respectively by absolute difference.

As seen in the above tables 4 and 5, although maldistribution is observed in the thermography, evaporation temperature can be predicted with the software as seen in figure 6. In this way, maldistribution is not degrading the performance in a high level. Contrarily, when the temperature difference in the secondary fluid is higher, the effect of maldistribution magnifies. This results in a general underperformance of the evaporator and of the global system.

For high temperature difference in the secondary fluid, evaporation temperature is unpredictable with a reliable software and opens the possibility to improve this kind of software with a new method to generate an initial guess of a better solution.

4. Conclusions

Maldistribution in a brazed plate heat exchanger has been experimentally observed with infrared thermography. When maldistribution occurs, evaporator surface temperature is distributed unevenly and can be registered with thermography as it is non-intrusive and non-contacting, having no influence in the evaporator. Inlet quality and superheat has been changed during the tests for a given water temperature difference to observe this phenomenon.

As observed in the thermography pictures, inlet quality has a great influence in maldistribution at first sight. For high inlet quality, better refrigerant distribution is observed. However, superheat is observed to have a minor effect. The higher the superheat, better distribution is shown in the thermography for a 5 K water temperature difference. Otherwise, an accumulation of two-phase flow is observed at the right side of the evaporator. Optimum refrigerant distribution is achieved when no superheat is performed.

Evaporation temperature has a great impact in system efficiency. Were the evaporator forced to work with a high level of superheat, less area is available for evaporation thus, evaporation temperature decreases. As expected, higher evaporation temperature is achieved when both low superheat and high inlet quality refrigerant is flowing. Although maldistribution is observed in thermography, underperformance is not inherited. Theoretical evaporation temperature obtained with reliable commercial software is compared with the obtained experimentally. Bigger temperature differences between experimental and theoretical results are obtained when higher temperature difference in the secondary fluid is present in the evaporator. The maldistribution effect is magnified by a higher temperature drop in the secondary fluid and penalizes the evaporator's correct operation.

5. Acknowledgements

Part of the results of this study were developed in the mainframe of the FP7 European project 'Next Generation of Heat Pumps working with Natural fluids' (NxtHPG). The authors would like to acknowledge the Spanish 'MINISTERIO DE ECONOMIA Y COMPETITIVIDAD', through the project ref-ENE2014-53311-C2-1-P-AR "Aprovechamiento del calor residual a baja temperatura mediante bombas de calor para la produccion de agua caliente" for the given support.

REFERENCES

- [1] BASSIOUNY, M K; MARTIN, H. *Flow distribution and pressure drop in plate heat exchangers—I U-type arrangement. Chemical Engineering Science* [online]. 1984, **39**(4), 693–700
- [2] BASSIOUNY, M K; MARTIN, H. *Flow distribution and pressure drop in plate heat exchangers—II Z-type arrangement. Chemical Engineering Science* [online]. 1984, **39**(4), 701–704
- [3] BOWERS, C D; WUJEK, S S; HRNJAK, P. *Quantification of Refrigerant Distribution and Effectiveness in Microchannel Heat Exchangers Using Infrared Thermography. Refrigeration And Air Conditioning*. 2010, (2006), 1–8.
- [4] BRIX, W; KÆRN, M R; ELMEGAARD, B. *Modelling refrigerant distribution in microchannel evaporators. International Journal of Refrigeration* [online]. 2009, **32**(7), 1736–1743
- [5] CORBERAN, J M; GONZÁLVIZ, J; MONTES, P; BLASCO, R; CORBERÁN, J M; GONZÁLVIZ, J; MONTES, P; BLASCO, R. 'ART' A Computer Code To Assist The Design Of Refrigeration and A/C Equipment. *International Refrigeration and Air Conditioning Conference*. 2002, (34), 1–8.
- [6] CORBERÁN, J M; DE CÓRDOBA, P F; GONZÁLVIZ, J; ALIAS, F. *Semiexplicit method for wall temperature linked equations (sewtle): A general finite-volume technique for the calculation of complex heat exchangers. Numerical Heat Transfer, Part B: Fundamentals* [online]. 2001, **40**(1), 37–59.
- [7] ELBEL, S; HRNJAK, P. *Flash gas bypass for improving the performance of transcritical R744 systems that use microchannel evaporators. International Journal of Refrigeration* [online]. 2004, **27**(7), 724–735
- [8] JENSEN, J K; KÆRN, M R; OMMEN, T; MARKUSSEN, W B; REINHOLDT, L; ELMEGAARD, B. *Effect of liquid/vapour maldistribution on the performance of plate heat exchanger evaporators. In: Refrigeration Science and Technology* [online]. 2015, s. 2007–2014
- [9] LONGO, G A. *Heat transfer and pressure drop during HFC refrigerant saturated vapour condensation inside a brazed plate heat exchanger. International Journal of Heat and Mass Transfer* [online]. 2010, **53**(5–6), 1079–1087
- [10] PITARCH, M; HERVAS-BLASCO, E; NAVARRO-PERIS, E; GONZÁLVIZ-MACIÁ, J; CORBERÁN, J M. *Evaluation of optimal subcooling in subcritical heat pump systems. International Journal of Refrigeration* [online]. 2017, **78**, 18–31

- [11] SWEP. SWEP distribution system. *SWEP Refrigerant handbook* [online]. [vid. 2019-01-17]. Dostupné z: <https://www.swep.net/refrigerant-handbook/6.-evaporators/asas5/>
- [12] THONON, B; MERCIER, P. *Les échangeurs à plaques: dix ans de recherche au GRETh: Partie 2. Dimensionnement et mauvaise distribution. Revue Générale de Thermique* [online]. 1996, **35**(416), 561–568
- [13] TUO, H; HRNJAK, P. *Effect of the header pressure drop induced flow maldistribution on the microchannel evaporator performance. International Journal of Refrigeration* [online]. 2013, **36**(8), 2176–2186
- [14] VIST, S; PETTERSEN, J. *Two-phase flow distribution in compact heat exchanger manifolds. Experimental Thermal and Fluid Science* [online]. 2004, **28**(2–3), 209–215
- [15] ZOU, Y; HRNJAK, P S. *Refrigerant distribution in the vertical header of the microchannel heat exchanger – Measurement and visualization of R410A flow. International Journal of Refrigeration* [online]. 2013, **36**(8), 2196–2208

Authors Index

- Álvarez Feijoo, M.A., 1277
Álvarez Gómez, P., 144
Álvarez Murillo, A., 989
Álvarez, C., 693, 702
Álvarez-Murillo, A., 1560
Álvarez-Piñeiro, L., 158, 167, 188
- Abánades-Velasco, A., 784
Abanades, A., 852
Abbas, R., 454, 1393, 1530
Acosta-Iborra, A., 795
Aguilar, F., 276, 1613, 1623
Aguilar, F.J., 978, 1198
Alaoui, F., 1623
Alarcón García, M., 336, 1323, 1333, 1553
Albadalejo, P., 265
Albaladejo, P., 188
Albaladejo-Hernández, D., 750
Albets, X., 1113
Aledo, S., 978
Almendros-Ibáñez, J.A., 475, 506, 590,
967, 1241, 1426, 1451
Alonso de Miguel, I., 559, 946, 1383
Alonso Tristán, C., 732
Alonso-Tristán, C., 946, 1277, 1628, 1637
Amat-Albuixech, M., 217, 229, 241
Amaya, A., 454
Aparicio Secanellas, S., 515
Aprea, C., 1101
Araiz, M., 150, 1360, 1523
Aranguren, P., 150, 1360, 1472, 1523
Arce Fariña, E., 732
- Arenas, E., 361
Arnaiz del Pozo, C., 414, 907, 1500
Arnaiz, C., 1371
Aroca, S., 1571
Astrain, D., 150, 1360
Atac Ylmaz, D., 312
Atienza-Márquez, A., 955
- Badia, J.D., 1285, 1292
Ballerini, C., 285
Ballester, S., 1285
Ballesteros, R., 605, 614
Barba, J., 605, 624
Barnes, M.J., 852
Barragán-Cervera, A., 229
Barreneche, C., 1426, 1666
Belmonte, J.F., 475, 590, 1241, 1451
Benayad, Z., 527
Benlloch-Dualde, J.V., 1461
Biedenbach, M., 1645
Blanco-Marigorta, A.M., 403
Boer, D., 15, 38, 807, 1155
Bou-Ali, M.M., 1657
Bourouis, M., 581, 1155
Bouzas, L., 1671
Brüggemann, D., 1645
Briongos, J.V., 1213
Bruno, J.C., 955
- Cánovas, M., 1478, 1484
Córcoles-Tendero, J.I., 590, 967
Cañada, M., 489

SPONSORS

